Comparison of Numerical Techniques for the Evaluation of Human Exposure From Measurement Data

Comparison of Numerical Techniques for the Evaluation of Human Exposure From Measurement Data

Alice Conchin Gubernati[1], Fabio Freschi[1], Luca Giaccone[1], Tommaso Campi[2], Valerio De Santis[2], and Ilkka Laakso[3]

[1]Dipartimento Energia "G. Ferraris", Politecnico di Torino, 10129 Torino, Italy
[2]Department of Industrial and Information Engineering and Economics, University of L'Aquila, 67100 L'Aquila, Italy
[3]Department of Electrical Engineering and Automation, Aalto University, 02150 Espoo, Finland

Numerical dosimetry makes it possible to evaluate the influence of electromagnetic fields on the human body. The interest of performing numerical dosimetry starting from data coming from general purpose software or measurements is constantly growing. This paper compares two available methods that make dosimetry starting from the knowledge of the magnetic flux density. The quality of results is analyzed considering both exact and uncertain inputs stressing out when one method should be preferred over the other. Finally, the methods are validated using real measurements obtaining good results.

Index Terms— **Computational electromagnetics, human exposure, low-frequency (LF) magnetic fields, magnetic measurements.**

I. Introduction

THE human exposure to electromagnetic fields coming from many different sources occurs in various situations due to the large diffusion of electric and electronic devices. Today, one of the key points is the simplification of dosimetric assessment procedure like, for example, enabling dosimetry starting from real measurements [1]–[3].

When considering low-frequency (LF) dosimetry, the scalar potential finite difference (SPFD) method is often the preferred one because the induced currents in the human body do not modify the source field and the problem can be formulated with the scalar potential as nodal unknowns [4]. Using the algebraic framework, the SPFD is given by [5]

$$\mathbf{G}^{\mathrm{T}}\mathbf{M}_{\sigma}\mathbf{G}\varphi = -\mathrm{j}\omega\mathbf{G}^{\mathrm{T}}\mathbf{M}_{\sigma}\mathbf{a}_{\mathrm{s}} \tag{1}$$

where, for a voxel human model, $\mathbf{M}_{\sigma}$ is a diagonal conductance matrix, $\mathbf{G}$ is the edge-to-node incidence matrix, and $\mathbf{a}_{\mathrm{s}}$ is the line integral of the magnetic vector potential (A-field) due to the sources [2].

The knowledge of the A-field is not straightforward when: 1) the software used to model the source does not provide the magnetic vector potential as output; 2) the model of the geometrical and the electrical layout of the source is very complex; and 3) no information is available about the source but only magnetic flux density (B-field) measurements. In all these cases, one can start from the knowledge of the B-field instead of the magnetic vector potential [1]–[3].

Recently, Arduino *et al.* [3] proposed a method that encloses the magnetic field source in a virtual box. The approach starts from the knowledge of the B-field on the external surface of this box. No real measurements have been considered but a huge number of virtual measurements have been used to estimate the uncertainty propagation. It is shown that this method has advantages over an alternative approach that starts from measurements inside the volume including the human body. If the magnetic field source is small (e.g., transcranical magnetic stimulation) the proposed approach is definitely a good option; however, for other sources, its application can be difficult (e.g., a power system substation) or impossible (e.g., an overhead power line). For this reason, this paper focuses on the strategy that starts from the knowledge of the B-field in a volume that includes the human body. The methods presented in [1] and [2] will be shortly described highlighting differences. A simple magnetic field source is selected to have reference simulation and also real measurements. Both methods are tested in order to point out strengths and weaknesses when the analysis starts from a simulated or measured B-field.

Manuscript received November 8, 2018; revised December 20, 2018; accepted January 26, 2019. Corresponding author: A. Conchin Gubernati (e-mail: alice.conchin@polito.it).

Color versions of one or more of the figures in this paper are available online at http://ieeexplore.ieee.org.

Digital Object Identifier 10.1109/TMAG.2019.2896720

II. Uncurl Methods Description

Hereinafter, we will refer to method 1 and method 2 to identify the approaches described in [1] and [2], respectively.

Method 1 is based on the knowledge of the B-field at discrete points in a bounded hexahedral grid. The components of the A-field are first obtained on the same grid by means of analytic formulas

$$\begin{aligned}
A_x &= -\int_0^y \left(\frac{1}{3}B_z(x,y',z)+\frac{1}{6}B_z(x,y',0)\right)dy' \\
&\quad +\int_0^z \left(\frac{1}{3}B_y(x,y,z')+\frac{1}{6}B_y(x,0,z')\right)dz' \\
A_y &= -\int_0^z \left(\frac{1}{3}B_x(x,y,z')+\frac{1}{6}B_x(0,y,z')\right)dz' \\
&\quad +\int_0^x \left(\frac{1}{3}B_z(x',y,z)+\frac{1}{6}B_z(x',y,0)\right)dx' \\
A_z &= -\int_0^x \left(\frac{1}{3}B_y(x',y,z)+\frac{1}{6}B_y(x',0,z)\right)dx' \\
&\quad +\int_0^y \left(\frac{1}{3}B_x(x,y',z)+\frac{1}{6}B_x(0,y',z)\right)dy'
\end{aligned} \tag{2}$$

then the A-field is interpolated on the computational domain to proceed with the classical SPFD scheme. A simple tri-linear interpolation of the A-field is sufficient to get very stable results. As a last remark, it is worth noting that the gauge applied to the magnetic vector potential coming from (2) is not known a priori because it depends on the arbitrary selection of the coordinate system (x, y, z) and its origin. This is not an issue because every compatible magnetic vector potential can be used in (1).

Method 2 is a topological approach defined within the algebraic framework. It allows to compute the circulation of the magnetic vector potential by solving the following system:

$$\begin{aligned} \mathbf{C}_R \mathbf{a}^c &= \mathbf{b}^{\text{free}} \\ \mathbf{a}^\tau &= 0 \end{aligned} \tag{3}$$

where $\mathbf{b}^{\text{free}}$ is a set of independent magnetic fluxes flowing through the voxel faces, $\mathbf{C}_R$ is the discrete curl incidence matrix restricted to the independent fluxes, and $\mathbf{a}^c$ and $\mathbf{a}^\tau$ are the cotree and tree circulations, respectively. $\mathbf{b}^{\text{free}}$, $\mathbf{a}^c$, and $\mathbf{a}^\tau$ are defined using the tree–cotree decomposition [6].

Method 2 is strictly related to the computational domain and this can be an advantage when the source B-field comes from simulations. In this case, one can directly compute $\mathbf{b}^{\text{free}}$ at the voxel faces. It is a disadvantage when the source B-field is known at discrete points. In this case, one must interpolate it to get $\mathbf{b}^{\text{free}}$ at the voxel faces. The interpolation of the B-field requires more attention to preserve the solenoidality. In the original study, a divergence-free interpolator based on Gaussian radial basis functions is proposed. In this paper, more details are given about the uncertainty propagation depending on the interpolation method and the type of input data.

III. Methodology

The exposure scenario considered in this paper is shown in Fig. 1(a). A five-turn coil with inner radius of 70 mm and wire radius of 3 mm is located 200 mm away from a square box. The side of the box is 300 mm. Each wire carries 1 A and the operating frequency is 1 kHz. The center of the coil corresponds to the origin of the reference system and the axis of the coil is the x-axis. The head of the Duke model (virtual family [7], voxel size $2 \times 2 \times 2$ mm^3) is centered in the square box and the coronal plane is the xz plane.

The exposure scenario is simple enough for simulations and also for the laboratory measurements as shown in Fig. 1(b). Measurements are performed with a NARDA commercial meter and the data are freely available at https://github.com/giaccone/Bfield_measured. Fig. 1(c) shows the measured B-field at 64 points. Reference solution is provided with direct calculation of the source B-field and A-field and with the simulation of the induced E-field [E_0, shown in Fig. 1(d)].

Methods 1 and 2 are used to test their performance by considering: 1) B-field coming from a simulation software and 2) B-field coming from measurements. In the latter case, several virtual measurements are generated to estimate the uncertainty propagation and true measurements are carried out to validate the two approaches. In all cases, the quality of the obtained result is taken into account using a relative error Δ defined as

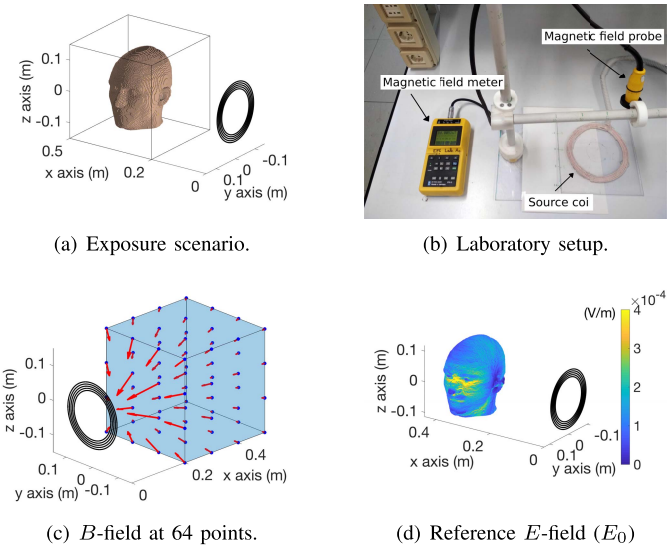

(a) Exposure scenario. (b) Laboratory setup.

(c) B-field at 64 points. (d) Reference E-field (E_0)

Fig. 1. (a) Exposure scenario considered in this paper. (b) Laboratory setup. (c) Measurement at discrete points with equal grid spacing along each directions. (d) Reference solution for the induced electric field.

$$\Delta = \sqrt{\sum_k \|\vec{\mathbf{F}}_k - \vec{\mathbf{F}}_{k,0}\|^2 \Big/ \sum_k \|\vec{\mathbf{F}}_{k,0}\|^2} \tag{4}$$

where $\vec{\mathbf{F}}_k$ is the magnetic or electric field at the kth voxel, whereas $\vec{\mathbf{F}}_{k,0}$ is the corresponding reference value.

IV. Numerical Analyses

In this section, it is considered that the input for both methods is a B-field coming from simulations. In Section IV-A, we consider the case when the magnetic field source is simulated with a specific software that is unable to perform the dosimetry step. Therefore, the B-field is exported and used with methods 1 and 2. In Section IV-B, we create virtual measurements to analyze the effect of a random noise superposed to the B-field. In Sections IV-A and IV-B, a large number of virtual measurements is considered in order to study the effects of the grid size. The measurements are generated on a regular grid with a regular grid size along each axis. The number of measurements varies from 64 to 10 648 points.

A. B-Field Coming From a Simulation Software

In a simple source configuration, the B-field can be computed exactly up to the machine tolerance. Both methods are adopted to invert the exact B-field discretized at a number of points from 64 to 10 648. Since method 2 requires the interpolation of the B-field, two procedures are tested: an interpolation with cubical splines and the divergence-free interpolator proposed in [2]. The results are shown in Fig. 2. All methods are used to compute the induced E-field in the head, and then the relative error is quantified. The relative error always decreases with the increase of the number of measurement points. Method 2 makes it possible to obtain the lowest relative error by means of the divergence-free interpolator even with little information about the B-field. A relative error of about

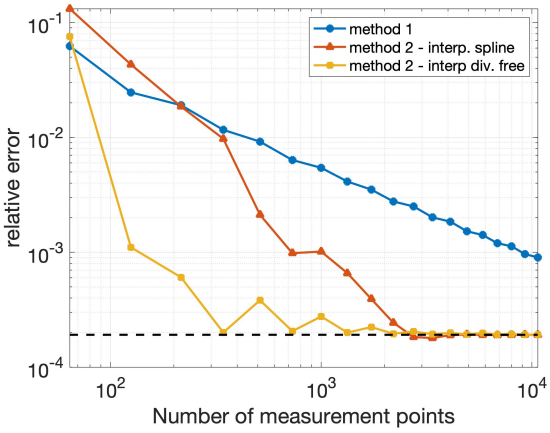

Fig. 2. Relative error of the induced E-field computed starting from the exact B-field.

10^{-3} is obtained with only 125 points. Furthermore, since method 2 is defined directly on the computational domain, the B-field could be exported directly at each center of the voxel faces. The black dashed line in Fig. 2 represents the relative error for this case (independent of the number of points). This is the best result that can be obtained with method 2 because it does not include the interpolation error. The same value cannot be quantified for method 1 because it must work first on a regular grid, and then it interpolates the magnetic vector potential on the computational domain.

For more than about 500 points, method 2 coupled with the divergence-free interpolation converges to the dashed line. This also means that more than 500 points are not necessary to get a very good accuracy. It is worth observing that above 500 points fluctuations of the relative error appear because the interpolation procedure is not yet preconditioned [8]. Finally, method 2 coupled with the spline interpolator should be avoided because it causes always a higher relative error.

B. Effect of the Noise on the B-Field

In this section, the exact B-field is computed, and then a random noise in the range 0–5% is superposed to the exact field. The maximum value of 5% is chosen in agreement with [3]. For each different number of points used to discretize the inspection volume: 1) 20 B-field distributions with noise are generated; 2) for method 2 only the relative error of the B-field interpolation is evaluated; and 3) the induced E-field is evaluated and the relative error is computed for both methods 1 and 2.

Fig. 3(a) shows the B-field interpolation error for method 2. It is immediately clear that the divergence-free interpolator is very sensitive to the random noise. In fact, the relative error dramatically increases with the number of measurement points (10, i.e., 1000%, with 10 648 points). The same sensitivity is not found for the spline interpolator that keeps the relative error in the same order of the random noise (i.e., 5%).

Fig. 3(b) shows the relative error on the E-field obtained using the B-field distributions previously described. SPFD method needs the circulation of the magnetic vector potential as right hand side of (1). This step involves an integral of the magnetic vector potential that has a smoothing effect of

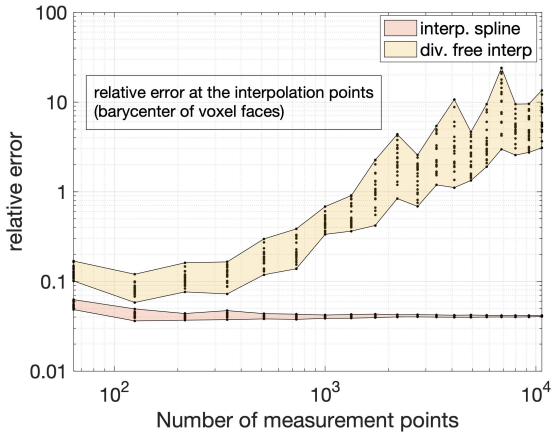

(a)

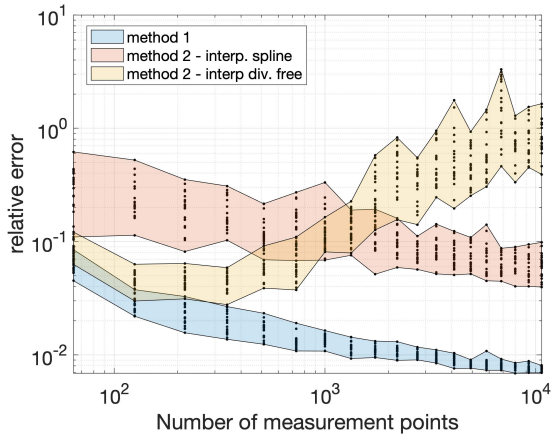

(b)

Fig. 3. (a) Relative error for the B-field interpolation performed for the use of method 2. (b) Relative error for the induced E-field.

the error on the B-field. In fact, the relative errors of the E-field are always lower than the related B-field [in Fig. 3(a)]. Method 1, whose curl inversion is based on an integration [see (2)], has a further smoothing effect that makes it not sensitive to the noise. For method 1, the error is always decreasing as the number of measurement points increases. The same trend is found for method 2 with the spline interpolator, however, the error is significantly higher than the one obtained with method 1. Therefore, the spline interpolator should be definitely avoided.

Regarding method 2 coupled with the divergence free interpolator, the relative error is acceptable in the first part of the plot but then increases again. This is due to the fact that the divergence-free interpolator is based on Gaussian radial basis functions, which constrain the interpolated B-field to be solenoidal. Gaussian radial basis functions work locally and, for higher number of points, the original B-field (that is not solenoidal due to the noise) is modified into a different solenoidal B-field distribution. This is the reason why the relative error is higher (for both B and E fields) when more measurement points are used. To sum up, method 2 coupled with the divergence free interpolator provides acceptable results (comparable with method 1) when the measurement grid for the B-field is not too dense, that is when the ratio

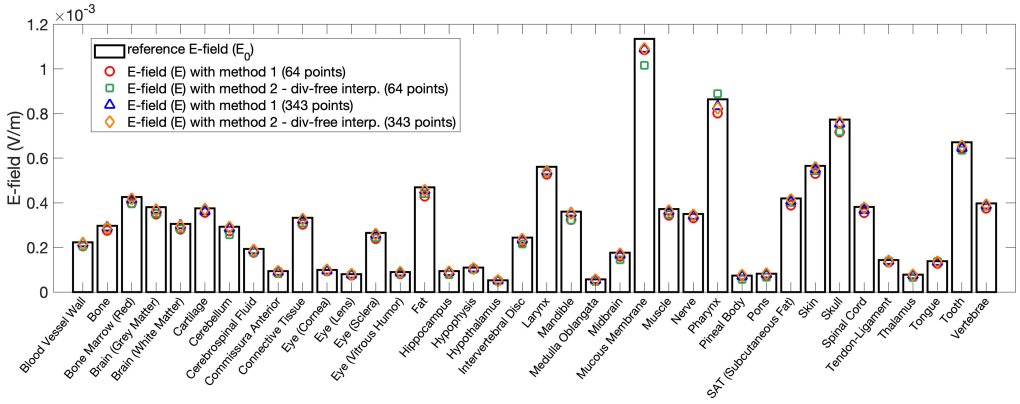

Fig. 4. Maximum value of the E-field at each tissue. Method 1 and method 2 are used starting from real measurements at 64 and 343 points. Results are compared with the reference case.

TABLE I
RELATIVE ERROR AND DEVIATION OF THE E-FIELD

Number of points	approach	Δ	E/E_0
64	method 1	0.08672	0.95607
	method 2 (div-free interp.)	0.10063	0.89511
343	method 1	0.03127	0.96102
	method 2 (div-free interp.)	0.03226	0.96190

between the grid spacing of the measurement grid and the side of the voxel is larger than 25 (i.e., low number of measurement points).

Bearing all this in mind, and considering that the measurement task is very time consuming, especially for complex sources [2], it is interesting the fact that an acceptable relative error can be obtained with few points (e.g., lower than 500).

V. EXPERIMENTAL ANALYSES

The two methods under comparison have been tested carrying out real measurements with the laboratory setup described in Section III, Fig. 1(b). Exploiting the results obtained in Sections IV-A. and IV-B., the B-field has been measured only at few points, 64 and 343. The E-field is computed with the SPFD method and possible numerical artifacts coming from the voxelized model are avoided by filtering the raw numerical solution with the 99.9th percentile approach [9]. Fig. 4 shows the results and it is apparent that both methods provide a good estimation of the E-field in all tissues. Table I summarizes the relative error of the numerical solution and the deviation at the tissue with maximum exposure (mucous membrane). The largest deviation, evaluated as E/E_0, is $\sim$0.9 (i.e., underestimation of 10%).

VI. CONCLUSION

This paper has analyzed two methods for calculating the magnetic vector potential starting from the knowledge of the magnetic flux density at discrete points. It is found that when the B-field comes from a simulation tool, method 2 coupled with a divergence free interpolator provides the most accurate results.

When the B-field is obtained through real measurements, method 1 is the preferred solution because it provides very stable results in any test condition. On the contrary, the use of method 2 requires more attention because a large number of measurement points could lead to higher errors.

This paper also shows that a huge number of measurement points is not necessary. It is found that if the ratio between the grid spacing of the measurement grid and the side of the voxel is higher than 25 the quality of the results is acceptable. In fact, when a cube with side of 300 mm is discretized with 64 or 343 points, very similar results are obtained. A maximum deviation of 10% is observed in the case of 64 points. Deviations in this order of magnitude are more than acceptable for a dosimetric assessment since other uncertainties (e.g., anatomical details, tissue properties,...) have the same order of magnitude.

REFERENCES

[1] I. Laakso, V. De Santis, S. Cruciani, T. Campi, and M. Feliziani, "Modelling of induced electric fields based on incompletely known magnetic fields," *Phys. Med. Biol.*, vol. 62, no. 16, 2017, Art. no. 6567.
[2] F. Freschi, L. Giaccone, V. Cirimele, and A. Canova, "Numerical assessment of low-frequency dosimetry from sampled magnetic fields," *Phys. Med. Biol.*, vol. 63, no. 1, 2018, Art. no. 015029.
[3] A. Arduino, O. Bottauscio, M. Chiampi, I. Laakso, and L. Zilberti, "Computational low-frequency electromagnetic dosimetry based on magnetic field measurements," *IEEE J. Electromagn., RF, Microw. Med. Biol.*, vol. 2, no. 4, pp. 302–309, Dec. 2018.
[4] T. W. Dawson and M. Stuchly, "Analytic validation of a three-dimensional scalar-potential finite-difference code for low-frequency magnetic induction," *Appl. Comput. Electromagn. Soc. J.*, vol. 11, no. 3, pp. 72–81, 1996.
[5] A. Canova, F. Freschi, L. Giaccone, and M. Manca, "A simplified procedure for the exposure to the magnetic field produced by resistance spot welding guns," *IEEE Trans. Magn.*, vol. 52, no. 3, Mar. 2016, Art. no. 5000404.
[6] R. Albanese and G. Rubinacci, "Finite element methods for the solution of 3D eddy current problems," *Adv. Imag. Electron Phys.*, vol. 102, pp. 1–86, Dec. 1997.
[7] A. Christ *et al.*, "The virtual family—Development of surface-based anatomical models of two adults and two children for dosimetric simulations," *Phys. Med. Biol.*, vol. 55, no. 2, pp. 23–38, 2010.
[8] G. E. Fasshauer and J. G. Zhang, "Preconditioning of radial basis function interpolation systems via accelerated iterated approximate moving least squares approximation," in *Progress on Meshless Methods* (Computational Methods in Applied Sciences), vol. 11, A. J. M. Ferreira, E. J. Kansa, G. E. Fasshauer, and V. M. A. Leitão, Eds. Dordrecht, The Netherlands: Springer, 2008, pp. 57–75.
[9] J. Gomez-Tames, I. Laakso, Y. Haba, A. Hirata, D. Poljak, and K. Yamazaki, "Computational artifacts of the *in situ* electric field in anatomical models exposed to low-frequency magnetic field," *IEEE Trans. Electromagn. Compat.*, vol. 60, no. 3, pp. 589–597, Jun. 2018.